

Distribution of α -AlFeSi and β -AlFeSi particles in surface layer of AA6063 alloy billets after heat treatment

Y. OSADA

Nikkei Analytical Center Ltd., 1-34-1 Kambara, Ihara-gun, Shizuoka-ken 421-3291, Japan
E-mail: chouta@thn.ne.jp

We developed the EPMA mapping method of small α -AlFeSi($\text{Al}_{8.3}\text{Fe}_2\text{Si}$) and β -AlFeSi($\text{Al}_{8.9}\text{Fe}_2\text{Si}_2$) particles in the billets of Al-Mg-Si alloys such as AA6063 alloys. To discriminate between α -AlFeSi and β -AlFeSi particles we used the relative X-ray intensities of Fe/Si ratio, the $I_{\text{Fe}}/I_{\text{Si}}$ ratio, instead of the Fe/Si mass ratio. To obtain the $I_{\text{Fe}}/I_{\text{Si}}$ ratio, we used a Monte Carlo method. In this study, using this method the mapping of α -AlFeSi and β -AlFeSi particles in the surface layer of AA6063 billets after the heat treatment (for 2 h at 580°C) was done. Namely, the distribution of α -AlFeSi and β -AlFeSi particles of zones from the billet surface to a depth of 800 μm was measured. Results showed the zone from the surface to a depth of 200 μm was occupied mainly by β -AlFeSi particles and the zone from a depth of 200 μm toward the center was occupied mainly by α -AlFeSi particles. From these results, it was found that if we remove zones from the surface to a depth of 200 μm , we can remove the majority of the β -AlFeSi particles, and thus improve the quality of anodizing performance of Al-Mg-Si alloys extrusions. © 2004 Kluwer Academic Publishers

1. Introduction

It is well known that in Al-Mg-Si alloys the spatial distribution and the spatial density of the particles of α -AlFeSi($\text{Al}_{8.3}\text{Fe}_2\text{Si}$) and β -AlFeSi($\text{Al}_{8.9}\text{Fe}_2\text{Si}_2$) particles [1], the size of which are larger than about 1 μm , affect the quality of anodizing performance of the final extrusions. For this reason, it is very important to control the spatial distribution and the spatial density of both types of AlFeSi particles at extrusion plants. Optical microscopes have been widely used to observe the distribution of those particles in AA6063 alloy billets, however it is not an appropriate method for identifying those particles. Also, the X-ray diffraction method (XRD) has been used for the discrimination between α -AlFeSi and β -AlFeSi particles. However, it is not appropriate method for determining the spatial distribution of particles. Recently, the surface layer of AA6063 alloy billets was measured with XRD [2]. However, we found that it is very difficult to make the specimen less than 1 mm thickness and now we are desired to determine the distribution of those particles in the surface layers. In this regard, the application of the electron probe analysis (EPMA) to the mapping of those particles is one of the most effective approach. In EPMA, we can do the quantitative analysis of α -AlFeSi and β -AlFeSi particles, however the quantitative analysis of the mapping is time consuming. It is not practically applicable to the mapping also if the particles are smaller than a generated X-ray region, the ZAF method cannot be used. From these viewpoints, the application of the Monte Carlo (MC) simulation to the mapping is one of

the most effective approaches. The Monte Carlo method for EPMA has been investigated for many years. Studies of the thickness determination of thin films [3, 4], the coefficient of backscattered electrons [5, 6], the generation of secondary electrons [7–9], and the quantitative analysis of small particles [10], have been reported. However, the Monte Carlo methods have not been applied to the discrimination between particles composed of the same element like α -AlFeSi and β -AlFeSi particles. Therefore, if we use the ratio of the characteristic X-ray intensities from main elements composed of α -AlFeSi and β -AlFeSi particles with MC simulation, we can do the mapping of those particles with EPMA. The aim of this study is to develop the mapping method of α -AlFeSi and β -AlFeSi particles of AA6063 alloy billets and using this mapping method we are to do the mapping of α -AlFeSi and β -AlFeSi particles in the surface layers of AA6063 alloy billets after heat treatment

2. Monte Carlo simulation

To calculate the characteristic X-ray intensities of α -AlFeSi and β -AlFeSi in the aluminum (matrix), we use a Monte Carlo simulation model. The Monte Carlo simulation model for electron scattering in a solid is shown in Fig. 1. As seen in the figure, an incident electron collides with one of the elements constituting a mixed target and is elastically scattered at an angle of (ω_n, ϕ_n) . The intensity of generated X-rays from the mixed target is calculated along the step length (λ_n). For the intensity of the generated X-rays, a self-absorption

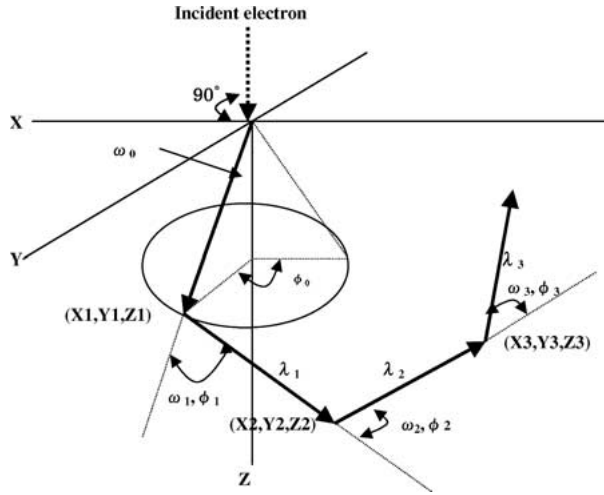


Figure 1 Scattering model of an electron.

effect is included, and an electron energy loss through one step is calculated. These calculations are carried out for all steps of each electron and the amount of the X-ray intensities is integrated. We use the screened Rutherford-type expression for elastic scattering of an incident electron. The scattering angle is determined using a uniform random number R as shown by Equation 1 [11]:

$$\cos \omega = 1 - 2\beta_i R / (1 + \beta_i - R), \quad (1)$$

where ω is the scattering angle (radian) of the electron and β_i the screening parameter which is described in the following section. A rotation angle ϕ is given by using another uniform random number R :

$$\phi = 2\pi R. \quad (2)$$

The probability (P_i) of an electron being scattered by i -th atom is given by Equation 3:

$$P_i = (\sigma_i \cdot EC_i/A_i) / \Sigma(\sigma_i \cdot C_i/A_i). \quad (3)$$

The total cross section (σ_{tot}^i) of the atom is given by Equation 4.

$$\sigma_{\text{tot}}^i = \rho N_{A\pi} e^4 \Sigma [C_i/A_i \cdot Z_i(Z_i + 1)] / [\beta_i(\beta_i + 1)] / 4E^2, \quad (4)$$

where A_i is the atomic weight, Z_i the atomic number, C_i the concentration in weight fraction, e the electron charge (-4.8029×10^{-10} esu), E (keV) the electron energy, N_A the Avogadro's number (6.02×10^{23}) and ρ (g/cm³) the mass density. Here $\beta_i = [5.44Z_i^{2/3}/E \times 10^{-3}]$ [12]. When an elastic collision occurs in a mixed target, we must consider which atom scatters the incident electron. The generated uniform random number R is shared as the proportional partition of the total cross section of each atom [11]. The expression is as follows for three elements of A , B and C . If $R \leq P_A$, then the electron collides with atom A . If $P_A < R \leq P_A + P_B$, the electron collides with atom

B . And if $P_A + P_B < R \leq P_A + P_B + P_C$, the electron collides with atom C .

The stopping power of an electron in a solid is given by Equations 5 and 6 [13, 14]. For $E > 6.338 \Sigma J_i C_i$,

$$\Delta E / \Delta S \text{ [keV/cm]} = 7.85 \times 10^4 \rho \Sigma [Z_i C_i / A_i \cdot \ln(1.166E/J_i)] / E. \quad (5)$$

For $E \leq 6.338 \Sigma J_i C_i$,

$$\Delta E / \Delta S \text{ [keV/cm]} = 7.85 \times 10^4 \rho \Sigma (Z_i C_i / A_i / J_i^{1/2}) / 1.26E^{1/2}, \quad (6)$$

where $\Delta E / \Delta S$ was the stopping power of the electron (ΔS represents a mean free path), and J_i the mean ionization potential; J_i [keV] = $11.5 Z_i \times 10^{-3}$ [15].

The characteristic X-ray intensity (I'_i) generated at the n -th step is given by Equation 7,

$$I'_i = N_A \rho Q_i(E) (W_i C_i / A_i) \lambda_n, \quad (7)$$

$$Q_i(E) E_{ik}^2 = 7.92 \times 10^{-20} \ln(U_i) / U_i,$$

$$U_i = E / E_{ik},$$

$$W_i = \alpha^4 / (1 + \alpha^4),$$

$$\alpha = -0.0217 + 0.032Z_i - 1.14Z_i^3 \times 10^{-5},$$

where $Q_i(E)$ [16] is the ionization cross section for inner shell electrons, λ_n the mean free path, E_{ik} (keV) the excitation energy of the K shell electron of an i -th atom, and W_i [17] the fluorescence yield. After this step, absorption correction of the X-ray intensity generated at the n -th step is carried out. Then, the relative X-ray intensity (I) are expressed as

$$I = I'_{An} / I'_{Sn} \quad (8)$$

where I'_{An} and I'_{Sn} are the X-ray intensities from an element A in the target and from the pure element A . The calculation of electron trajectories is stopped either when the electron escapes from the targets into the vacuum or when the electron energy falls to below the critical excitation energy. The big feature of this MC simulation is to be able to obtain results with enough accuracy for a few minutes with a commercial type personal computer. This MC code has been already described in detail [18, 19]. Also, the elastic scattering and the inelastic scattering regarding the samples such as compounds, alloys, mixed targets and multiple layers have been described in [11].

The targets used in this study are very small, for this it is necessary to consider that we assume the shape of targets used in the MC calculation. The geometrical shapes of α -AlFeSi and β -AlFeSi are commonly observed as a plate shape and a needle shape, respectively. Therefore the shape of particles of α -AlFeSi and β -AlFeSi in aluminum (matrix) was assumed to be a rectangular parallel piped. The schematic of α -AlFeSi and β -AlFeSi particles in the aluminum matrix employed in the present MC model is shown in Fig. 2. Since the particles larger than 1 μm are important in

TABLE I Parameters used for Al, Fe and Si, K_{α} lines

Element (Line)	Critical excitation voltage (keV)	Atomic number	Atomic weight	Absorption coefficient
Al (K_{α})	1.559	13	26.98	Al \rightarrow Al 407
				Al \rightarrow Fe 3420
				Al \rightarrow Si 552
Fe (K_{α})	7.11	26	55.847	Fe \rightarrow Fe 76
				Fe \rightarrow Al 99
				Fe \rightarrow Si 124
Si (K_{α})	1.838	14	28.08	Si \rightarrow Al 3440
				Si \rightarrow Fe 2490
				Si \rightarrow Si 360

TABLE II Parameters used for AlFeSi particles, Al, Fe, Si

Targets	Atom	Mass%	Density (g/cm^3)
α -AlFeSi	Al	62.0	3.5
	Fe	30.0	
	Si	8.0	
β -AlFeSi	Al	58.0	3.5
	Fe	27.0	
	Si	15.0	
Element	Fe	100	7.86
	Al	100	2.7
	Si	100	2.34

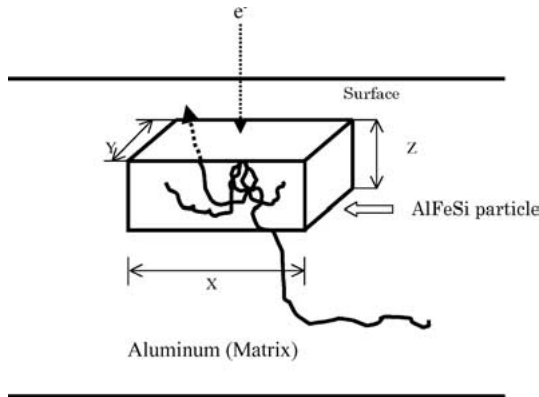


Figure 2 Schematic of an AlFeSi particle in the aluminum matrix employed in MC calculation.

practice, the minimum of the particle size was assumed to be $x = y = z = 1 \mu\text{m}$. The maximum size was assumed to be $x = y = z = 10 \mu\text{m}$, which can be regarded as bulk. The particles were assumed to locate at the sample surface and incident electrons impinged at the center of the particle surface. The take off angle of X-ray is 52.5° from the sample surface.

3. Results and discussions

3.1. Relative X-ray intensity

By using MC code as mentioned Section 2, we calculated the characteristic X-ray (K_{α}) intensities of Al,

Fe and Si generated from each pure element, and from α -AlFeSi and β -AlFeSi particles which sizes are $x = y = z = 1 \mu\text{m}$ and $x = y = z = 10 \mu\text{m}$. The initial energy of the electron was 15 keV. The numbers of incidence electron were 150. The incidence angle was 0° (normal incidence) and the take angle of X-ray was 52.5° . Table I shows parameters for Al, Fe and Si used in the MC calculation. Table II shows the mass% and the density of those particles. The variation of MC calculation was estimated by statistical errors of ten trials obtained by changing the initial value for random number generation. The particles used in calculations were α -AlFeSi ($\text{Al}_{8.3}\text{Fe}_2\text{Si}$) and β -AlFeSi ($\text{Al}_{8.9}\text{Fe}_2\text{Si}_2$). The X-ray intensities generated from particles were converted into the relative X-ray intensities by Equation 8. Table III shows the calculated results of the relative X-ray intensities, I_{Al} , I_{Fe} and I_{Si} from each AlFeSi particle.

3.2. Discrimination between α -AlFeSi and β -AlFeSi Particles

Fig. 3a and b show the calculated results for I_{Fe} and I_{Si} of α -AlFeSi and β -AlFeSi targets in Table III. The circle and diamond in figures show the results of sizes of $x = y = z = 1 \mu\text{m}$ and $x = y = z = 10 \mu\text{m}$, respectively. As seen in Fig. 2, if the I_{Fe} and the I_{Si} are smaller than those of the size of $x = y = z = 1 \mu\text{m}$, namely if the I_{Fe} and the I_{Si} are smaller than 0.2123 and 0.0343, respectively, they are assumed to be matrix, if more than those, they are assumed to be particles. Fig. 4 shows the calculated results for $I_{\text{Fe}}/I_{\text{Si}}$ ratio of α -AlFeSi and β -AlFeSi in Table III. The circle and diamond in the figure show results for the sizes of $x = y = z = 1 \mu\text{m}$ and $x = y = z = 10 \mu\text{m}$, respectively. From the Fig. 4, it was found that the $I_{\text{Fe}}/I_{\text{Si}}$ was 4 or more for α -AlFeSi and less than 4 for β -AlFeSi [18].

3.3. Mapping method

Fig. 5 shows the flow sheet to discriminate between α -AlFeSi and β -AlFeSi particles. Using this flow sheet, we developed the mapping program of α -AlFeSi and β -AlFeSi particles for EPMA 8705 sited at Shimadzu Corporation. This mapping program, written in BASIC language, can automatically measure the distribution of α -AlFeSi and β -AlFeSi particles. First, we measured the X-ray (K_{α}) intensities of Fe and Si from each pure element, secondly we measured the X-ray (K_{α}) intensities of Fe and Si from analytical points divided like a mesh in the sample. After that, the X-ray intensities obtained from each analytical point were converted into the relative X-ray intensities automatically and each analytical point was decided whether matrix or particles

TABLE III Calculated results of I_{Al} , I_{Fe} and I_{Si} from each AlFeSi particle

Samples	Size: $x = y = z = 1 \mu\text{m}$			Size: $x = y = z = 10 \mu\text{m}$		
	I_{Al}	I_{Fe}	I_{Si}	I_{Al}	I_{Fe}	I_{Si}
α -AlFeSi	0.6863 ± 0.0172	0.2397 ± 0.0035	0.0378 ± 0.0035	0.5211 ± 0.0011	0.2771 ± 0.0049	0.0516 ± 0.0011
β -AlFeSi	0.6675 ± 0.0248	0.2183 ± 0.0060	0.0717 ± 0.0046	0.4839 ± 0.0111	0.2460 ± 0.0053	0.0973 ± 0.0032

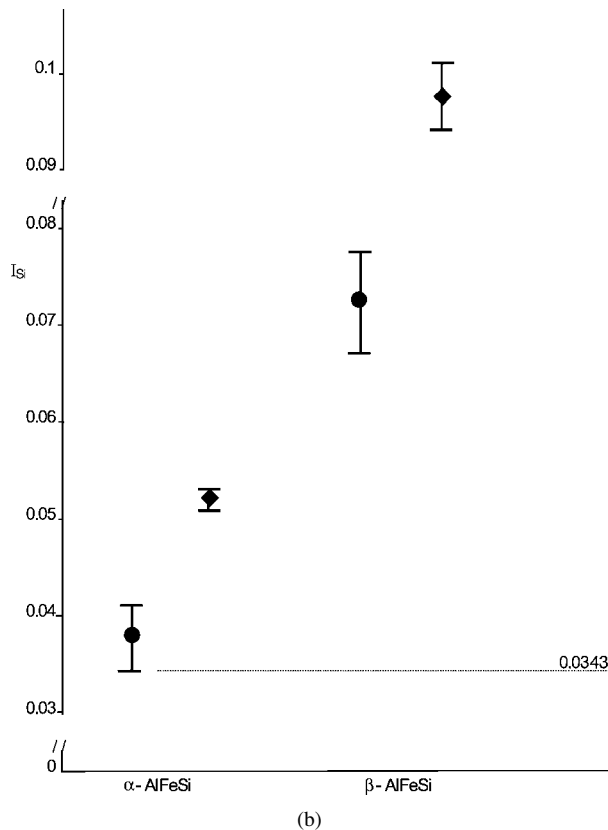
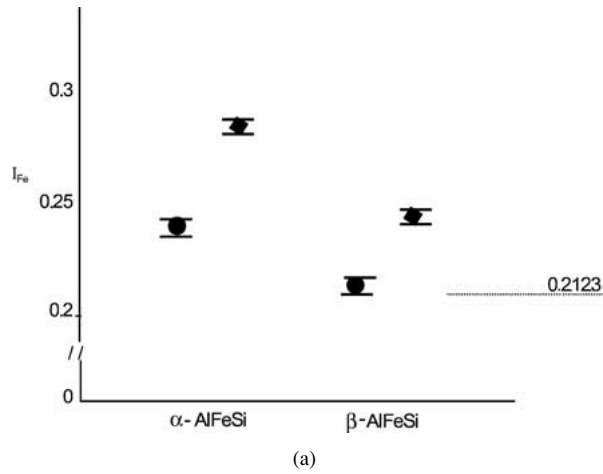


Figure 3 (a) Relative X-ray intensity (I_{Si}) of Si from α -AlFeSi and β -AlFeSi targets (●: the size of $x = y = z = 1 \mu\text{m}$, ◆: the size of $x = y = z = 10 \mu\text{m}$) and (b) Relative X-ray intensity (I_{Si}) of Si from α -AlFeSi and β -AlFeSi targets (●: the size of $x = y = z = 1 \mu\text{m}$, ◆: the size of $x = y = z = 10 \mu\text{m}$).

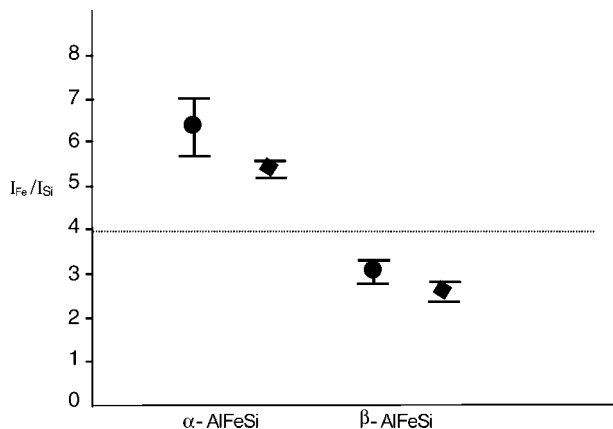


Figure 4 I_{Fe}/I_{Si} of Fe from α -AlFeSi and β -AlFeSi targets (●: the size of $x = y = z = 1 \mu\text{m}$, ◆: the size of $x = y = z = 10 \mu\text{m}$).

TABLE IV Chemical composition of AA6063 billet mass(%)

Fe	Si	Mg	Cu	Ti	Mn	Ni	Zn	Cr	Al
0.18	0.40	0.50	0.010	0.010	0.006	0.004	0.006	0.003	Bal.

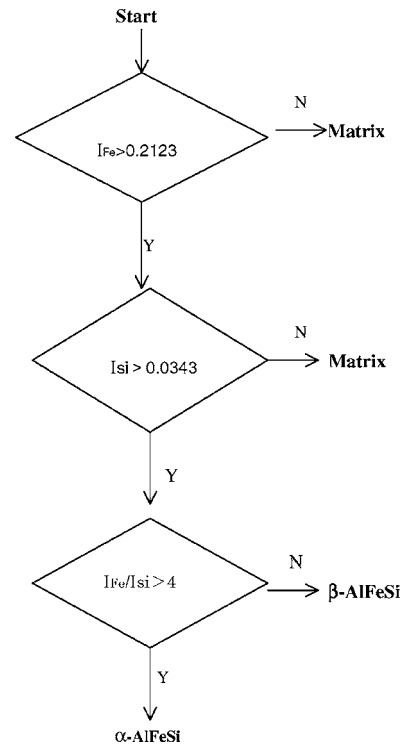


Figure 5 Flow sheet to discriminate between α -AlFeSi and β -AlFeSi targets.

judging from the flow sheet. Finally the images of those particles displayed in different colors on a CRT.

3.4. Results of mapping

We used a wavelength dispersive EPMA-8705 spectrometer (Shimadzu corporation, X-ray take off angle of 52.5°). The measurement was done with electron-beam current 20 nA, at accelerating voltage of 15 kV and at angle of incidence 0° (normal incidence). Samples ($10 \text{ mm} \times 10 \text{ mm} \times 10 \text{ mm}$) was cut off from the billet surface to inside were heat-treated for 2 h at 580°C and then embed in resin and polished with diamond paste. Additionally, we prepared Fe (4N) and Si (4N). Also, the chemical composition of AA6063 alloy billets is shown in Table IV. Furthermore, in order to carry out night-time determinations, a measurement time of 0.5 s/pixel, the analysis area $400 \times 400 \mu\text{m}^2$ and the pixel number 200×200 were set. The zone from the surface to a depth of $400 \mu\text{m}$ and the zone from a depth of $400 \mu\text{m}$ to a depth of $800 \mu\text{m}$ were measured. Fig. 6 shows the results of the mapping. In the figure, the red contrast means α -AlFeSi particles and the green contrast means β -AlFeSi particles. Fig. 6a shows the result of the mapping of the zone from the surface to a depth of $400 \mu\text{m}$. Fig. 6b shows the result of the mapping of the zone from a depth of $400 \mu\text{m}$ to a depth of $800 \mu\text{m}$. As a result, from the Fig. 6a, the zone from the surface to $200 \mu\text{m}$ inside was occupied mainly

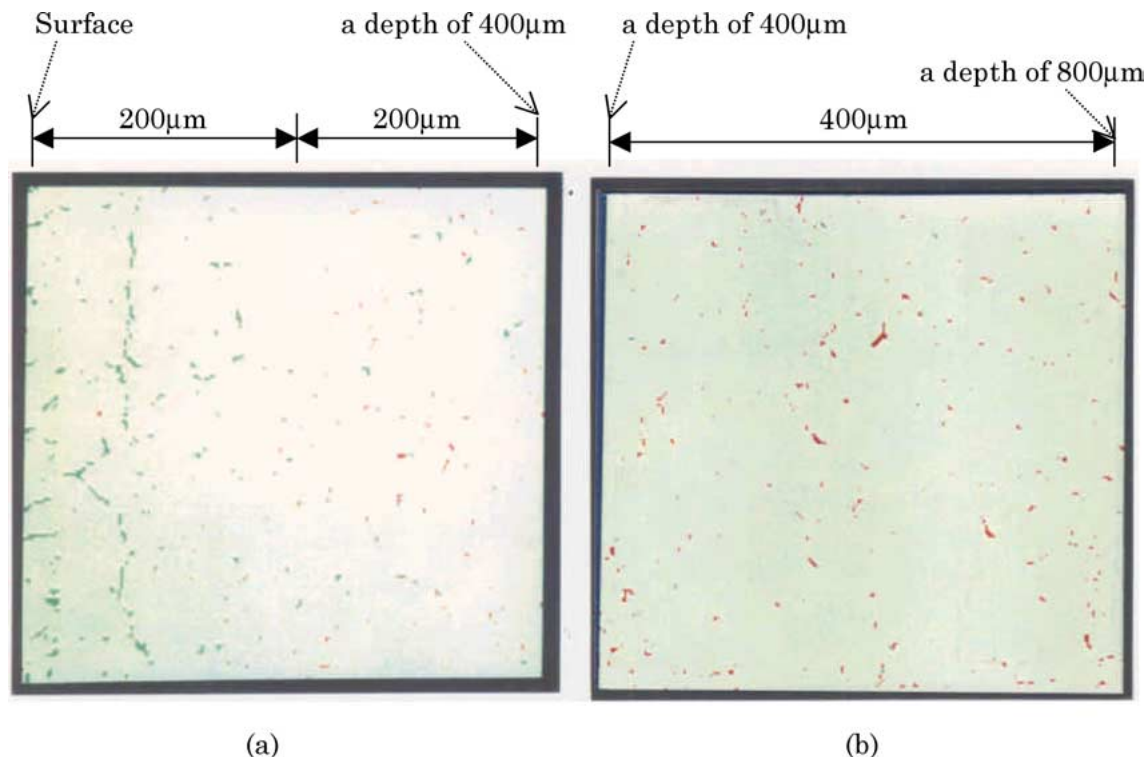


Figure 6 Mapping of α -AlFeSi and β -AlFeSi particles from the surface layer to a depth of 800 μm .

by β -AlFeSi particles and β -AlFeSi particles gradually decreased with an increase of α -AlFeSi particles in the zone from a depth of 200 μm to a depth of 400 μm . From the Fig. 6b, the zone from a depth of 400 μm to a depth of 800 μm was occupied mainly by α -AlFeSi particles.

4. Conclusion

In this paper, the EPMA mapping method applies to the mapping of α -AlFeSi and β -AlFeSi particles in the surface layer of AA6063 billets. As a result, in spite of the practical operation heat treatment (for 2 h at 580°C), the segregation zone from the billet surface to a depth of 200 μm is occupied mainly by β -AlFeSi particles. The zone from a depth of 200 μm toward the center is occupied mainly by α -AlFeSi particles. From this, it was found that if we remove the surface layers to a depth of 200 μm , we can remove the majority of the β -AlFeSi particles, and thus improve the quality of the anodizing performance after the billet is extruded.

Acknowledgments

The author wishes to thank Professor Kenji Murata of Osaka Prefecture University for his valuable suggestions on Monte Carlo calculation and Also, the author wishes to thank metallurgist Shuichiro Watanabe for his metallurgical suggestions and Mr. Hiroshi Nagashima of Research and Development Center of Nippon Light Metal Co. Ltd. for supplying the reference samples.

References

1. G. RIVLIN and G. V. RAYNOR, *Intern. Met. Rev.* **3** (1981) 133.
2. T. MINODA, H. HAYAKAWA and H. YOSHIDA, Meeting of Japan Institute of Light Metals in Spring (1997) (Journal of Japan Institute of Light Metals)
3. K. MURATA, M. KOTERA and K. NAGAMI, *J. Appl. Phys.* **54**(2) (1983) 1110.
4. N. AMMANN and P. KARLUCK, *Surf. Interf. Analysis* **22** (1994) 54.
5. P. G. T. HOWELL and A. BOYDE, *Scanning* **20** (1998) 45.
6. K. MURATA, *J. Appl. Phys.* **45**(9) (1974) 4110.
7. K. MURATA, D. F. KYSER and C. H. TING, *ibid.* **52**(7), (1981) 4396.
8. H. SEILER, *ibid.* **54** (1983) R1.
9. DING ZE-JUN and R. SHIMIZU, *Scanning* **18** (1996) 92.
10. K. OOBORI, R. SHIMIZU, T. OURA and S. ICHIKAWA, *J. Appl. Phys.* **54**(1) (1983) 150.
11. K. MURATA, T. MATSUKAWA and R. SHIMIZU, in Proceeding of the Sixth International Conference on X-ray Optics Microanalysis, Tokyo (1972) p. 105.
12. B. P. NIGAM, M. K. SAUNDERSON and WU. TA-YOU, *Phys. Rev.* **115** (1959) 491.
13. H. A. BETHE, *Ann. Physik (Leipzig)* **5** (1930) 325.
14. T. RAO-SAHIB and D. B. WITTRY, *J. Appl. Phys.* **45** (1974) 5060.
15. R. WILSON, *Phys. Rev.* **60** (1941) 749.
16. M. GREEN and V. E. COSSLETT, *Proc. Phys. Soc.* **78** (1961) 1206.
17. J. LABERRIGUE-FROLOW and P. RADVANYI, *J. Phys. Radium* **17** (1956) 944.
18. Y. OSADA, *J. Materials Science* **38** (2003) 1457.
19. *Idem.*, X-RAY Spectrometry (2003, in press).

Received 2 May
and accepted 13 October 2003